López-Puente, J., Mata-Díaz, A., Pernas-Sánchez, J., Artero-Guerrero, J. A., & Varas, D. (2018). Numerical study of composite fragment impacts onto rigid target. Composite Structures, 203, 172-181.

doi:https://doi.org/10.1016/j.compstruct.2018.07.002

Numerical study of composite fragment impacts onto rigid target

J. López-Puente[a], A. Mata[b], J. Pernas-Sánchez[a], J. A. Artero-Guerrero[a], D. Varas[a]

[a] *Department of Continuum Mechanics and Structural Analysis. Universidad Carlos III de Madrid. Avda. de la Universidad, 30. 28911 Leganés, Madrid, Spain*
[b] *Gestamp Servicios SA. Calle Alfonso XII 16. 28014 Madrid, Spain*

Abstract

In this work, it is proposed a numerical methodology to model the behaviour of composite laminates when they act as impactors at high velocity. The numerical model uses an intralaminar criterion based in the Hashin model and a Progressive Damage model to describe the ply behaviour, whereas the interlaminar failure is taken into account by means of cohesive interactions. The validation of the model is performed attending the kinematics and erosion of the laminate during the impact process onto a rigid target as well as the force and impulse generated. Once validated, the model is used to analyse the influence of the fragment miss-alignment in the impact process.

Keywords: composite, fragment, high-velocity impact, numerical, Progressive damage analysis, Hashin model

1. Introduction

The reduction in fuel consumption of the commercial aircraft is achieved, mainly, because of the structure lightening and the improvement of the engines. In both cases composite laminates play a very important role, since they exhibit outstanding specific mechanical properties. The main drawback of CFRPs (from the structural point of view) is the poor performance against impact when it occurs perpendicularly to the laminate plane. Understanding the behaviour of laminates subjected to that kind of impacts is of great importance since the

use of those materials (in particular carbon/epoxy, CFRP) in aircraft structures has reached approximately 50% (in terms of weight).

Composite laminates are increasingly used in aircraft engines, both in the fan blades and in the engine case, which in case of an uncontained failure, could impact the CFRP fuselage. In addition the new open-rotor engines, which probably will propel future aircrafts, use counter rotating blades, without fan case protection, manufactured using composite laminates that also could impact the fuselage in case of failure. In the framework of the CleanSky 2 program (which belongs to the Horizon 2020 program of the European Commission) there is an activity with the objective of demonstrate the performance of this new engine. One of the main challenges is the need of protection of the aircraft fuselage against the possible impact of one of those blades. Those examples show the importance of studying the behaviour of carbon/epoxy laminates acting as impactors at high velocity.

The behaviour of composite laminates under dynamic loading conditions (as a structural component) has received relevant attention from many authors. The failure mechanisms and the influence on the CFRP response of different variables such as impact velocity [1], projectile geometry, projectile obliquity or temperature have been widely analysed experimentally [1–3]. In addition, researchers have made a great effort on developing numerical models to reproduce the different damage mechanisms that appear in laminates under impact conditions studying the influence of different projectile shapes, obliquity or materials using different approaches [4–15].

The analysis of how a composite fragment behaves as an impactor at high velocity has received almost no attention from other researchers. The most similar works are those which studied the crushing of composite tubes. In this field it is possible to find some static analysis and also studies of tubes reinforced with foams or even aluminium. Mamalis et al. [16, 17] analysed the dynamic compression of pure CFRP tubes from a numerical and experimental point of

view. The main objective of those works was related to the study of the energy absorbed during the crushing process. Recently H.A.Israr et al. [18, 19] published interesting studies, both experimental and numerical, regarding the laminates crushing. They show the failure process of the laminate during the impact, being able to identify the different failure modes involved in the process. It is worth to say that the last mentioned works study quasi-static cases and low velocity impacts as well as that the specimens were cut to form a chamfering-type trigger mechanisms. The failure mechanisms and the impact process of a laminate without chamfer impacting at high velocity could be different.

The authors of the current work have studied this type of impact, from the experimental point of view [20], launching composite fragments by means of a pneumatic launcher in a range of impact velocities between 70 to 180 m/s. Prior to perform an impact of a composite fragment against a composite panel, it was considered more interesting to carry out a simpler test in order to study the failure mechanisms that appear in the CFRP fragment during the impact. The impact force that a composite fragment at high velocity induces is of great interest for the aircraft industry in order to design structures that could withstand such kind of loads. The force induced by the impact of a composite fragment will depend on the flexibility of the structure where impacts; as the flexibility increases, the force diminishes. When the fragment impacts a rigid plate, the force induced will be the highest possible, and hence it could be considered the worst-case scenario.

The objective of this work is to develop a numerical methodology to predict the behaviour of carbon/epoxy unidirectional fragments when impacting a rigid plate in a range of velocities between 70 to 180 m/s. The numerical model uses an intralaminar criterion based in the Hashin model and a Progressive Damage model to describe the ply behaviour, whereas the interlaminar failure is taken into account by means of cohesive interactions. The validation of the model is performed attending the kinematics and erosion of the laminate during the impact process onto a rigid target, as well as the force and impulse generated. The

experimental results are obtained from a previous work of the current authors [20]. Once validated, the model is used to analyse the influence of the fragment miss-alignment in the impact process.

Although there are numerous numerical works dealing with the modelling of laminates, it was not possible to find any numerical work regarding the analysis of a composite laminate impacting at high velocity against other surface. Therefore developing a numerical methodology capable of reproduce this kind of impacts or even reaching some conclusion about which kind of failures should be taken into account in the model, could be of great interest.

2. Material modelling

In order to predict the behaviour of unidirectional composite fragments impacting at high velocity, a numerical methodology has been developed using the commercial explicit finite element code Abaqus/Explicit v6.12. This software has been specifically designed to simulate dynamic events with important non-linearities (material and geometrical), which both appear in the problem studied in the current work.

In order to model the behaviour of a unidirectional composite laminate is necessary to use a intra-laminar failure criteria to describe the failure inside the plies, and a inter-laminar model to define the behaviour between the plies. To obtain precise results, the model should consider all the laminate plies and every inter-ply. In the following sections, the material modelling is described.

2.1. Intra-laminar failure and damage evolution

The composite laminate behaves as an orthotropic elastic material until damage starts. The Hashin and Rotem model [21] has been used to model the intra-laminar failure; this material is already implemented in the software material

library, to be used with shell (or continuum shell) elements. The aforementioned model is implemented in the code using a progressive damage analysis that is a generalization of the approach proposed by Camanho and Davila [22]. In this section a brief description of the model is performed; further details could be found in the software documentation [23]. In this model, the onset of damage is defined by the Hashin and Rotem damage initiation criteria [24], which adequately predicts the different intra-laminar failure mechanisms. Once it occurs, the damage will evolve degrading the material stiffness coefficients until the energy dissipated is equal to the fracture toughness (divided by the element characteristic length), when the material is fully damaged. Four different uncoupled damage initiation criteria are defined as follows:

- Fibre failure under tension ($\hat{\sigma}_{11} \geq 0$)

$$F_t^f = \left(\frac{\hat{\sigma}_{11}}{X_T}\right)^2 + \alpha \left(\frac{\hat{\sigma}_{12}}{S_L}\right)^2 \tag{1}$$

  where $\hat{\sigma}_{ij}$ are the components of the effective stress tensor (with no damage) proposed by Matzenmiller et al. [25], X_T and S_L are the tensile (in the fibre direction) and in-plane shear strengths of the laminate, and α is a parameter that allows to calibrate the contribution of the in-plane shear stress in the failure criterion. In order to not overestimate the contribution of the in-plane stress, the parameter α must be less or equal than 1, and positive. In this case its value is $\alpha = 1$.

- Fibre failure under compression ($\hat{\sigma}_{11} < 0$)

$$F_c^f = \left(\frac{\hat{\sigma}_{11}}{X_C}\right)^2 \tag{2}$$

  where X_C is the compressive strength of the laminate in the fibre direction.

- Matrix failure under tension ($\hat{\sigma}_{22} \geq 0$)

$$F_t^m = \left(\frac{\hat{\sigma}_{22}}{Y_T}\right)^2 + \alpha \left(\frac{\hat{\sigma}_{12}}{S_L}\right)^2 \tag{3}$$

Property	**Symbol**	**Magnitude**	**Units**
Density	ρ	1580	kg/m^3
Young modulus 0°	E_1	135	GPa
Young modulus 90°	E_2	9.6	GPa
In-plane shear modulus	G_{12}	4.5	GPa
Out-plane shear modulus	$G_{13} = G_{23}$	5.3	GPa
Poisson coefficient 12	ν_{12}	0.32	–
Compressive strength 0°	X_C	1531	MPa
Tensile strength 0°	X_T	2207	MPa
Compressive strength 90°	Y_C	158	MPa
Tensile strength 90°	Y_T	73	MPa
In-plane Shear strength	S_L	114.5	MPa
Out-of-plane Shear strength	S_T	102.3	MPa
Ply tensile fracture energy 0°	G_{1+}	81.5	kJ/m^2
Ply compression fracture energy 0°	G_{1-}	106.3	kJ/m^2
Ply tensile fracture energy 90°	G_{2+}	0.28	kJ/m^2
Ply compression fracture energy 90°	G_{2-}	1.313	kJ/m^2

Table 1: Carbon epoxy AS4/8552 properties from the manufacturer Hexcel and literature [26, 27]

where Y_T is the tensile strength of the laminate in the matrix direction.

- Matrix failure under compression ($\hat{\sigma}_{22} < 0$)

$$F_c^f = \left(\frac{\hat{\sigma}_{22}}{2S_T}\right)^2 + \left[\left(\frac{Y_C}{2S_T}\right)^2 - 1\right]\frac{\hat{\sigma}_{22}}{Y_C} + \left(\frac{\hat{\sigma}_{12}}{S_L}\right)^2 \tag{4}$$

where Y_C and S_T are the compressive (in the matrix direction) and out-of-plane shear strengths of the laminate.

All the material properties, shown in table 1, are obtained from the literature and the manufacturer data-sheet.

Once any of the failure initiation criteria reaches the value of one, any addi-

tional strain increment will reduce the values of stiffness of the element in the corresponding direction following a linear evolution law (Fig.1). This decrease depends on the energy dissipated during the process (see work of Turon et al. [28]), since the area under the triangle should be equal to the material fracture toughness divided by the element characteristic length.

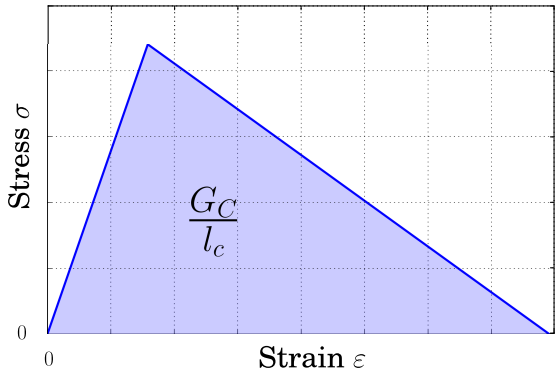

Figure 1: Linear damage evolution.

Each damage initiation mechanism has its own damage variable that controls the stiffness degradation, and its value goes from zero (undamaged) to one (fully damaged). The stiffness tensor C_d, that relates the stress and the strain (written in vectorial form) is:

$$C_d = \begin{pmatrix} \frac{(1-d_f)E_1}{g} & \frac{(1-d_f)(1-d_m)\nu_{21}E_1}{g} & 0 \\ \frac{(1-d_f)(1-d_m)\nu_{12}E_2}{g} & \frac{(1-d_m)E_2}{g} & 0 \\ 0 & 0 & (1-d_s)G_{12} \end{pmatrix} \tag{5}$$

where $g = 1-(1-d_f)(1-d_m)\nu_{12}\nu_{21}$, E_i are the Young modulus in each direction, ν_{12} *and* ν_{21} are Poisson's ratios, G_{12} is the in-plane shear modulus and the damage variables are d_m for the matrix direction, d_f for the fibre direction and d_s for the shear; the aforementioned damage variables are defined as a

function of the displacement of the nodes, further information could be found in the software documentation [23]. When a damage variable reaches the value of one, the stiffness is fully degraded in the corresponding direction keeping constant and equal to zero the associated stress component.

2.2. Inter-laminar failure

In order to model the interaction between the plies, a cohesive interaction approach has been used to take into account the inter-laminar behaviour and failure. The cohesive interaction has an advantage compared to the cohesive element in this type of problems since no distortion could occur. The cohesive behaviour is based on a traction-separation law, in which is necessary to define a damage initiation criterion and a damage evolution law. The damage initiation is defined by means of a quadratic nominal stress criterion defined as follows:

$$\left\{\frac{\langle t_n \rangle}{t_n^o}\right\}^2 + \left\{\frac{t_s}{t_s^o}\right\}^2 + \left\{\frac{t_t}{t_t^o}\right\}^2 = 1 \tag{6}$$

where t_n, t_s and t_t represent the values of the nominal stress when the deformation is purely normal to the interface, in the first shear direction or in the second shear direction, respectively, and t_n^o, t_s^o and t_t^o are their strengths.

The damage evolution law is defined by means of a scalar variable (D) function of the separation between the surfaces which degrades the contact stress components:

$$\begin{aligned} t_n &= \begin{cases} (1-D)\bar{t}_n, & \bar{t}_n \geq 0 \\ \bar{t}_n \end{cases} \\ t_s &= (1-D)\bar{t}_s \\ t_t &= (1-D)\bar{t}_t \end{aligned} \tag{7}$$

where $\bar{t}_n$, $\bar{t}_s$ and $\bar{t}_t$ are the contact stress components predicted by the elastic traction-separation behaviour for the current separations without damage. This degradation produces a linear decay of the stress-traction curve.

Property	**Symbol**	**Magnitude**	**Units**
Nominal stress in mode I (Purely normal)	t_n^0	80.7	MPa
Nominal stress in mode II & III (Shear direction)	$t_s^0 = t_t^0$	114.5	MPa
Coefficient in mixed mode	η	1.45	
Energy release rate in mode I (Purely normal)	G_n^c	0.25	kJ/m^2
Energy release rate in mode II (Shear direction)	G_s^c	0.791	kJ/m^2

Table 2: Cohesive interaction parameters.

The mixed mode has been taken into account using the criterion proposed by Benzeggagh and Kenane [29], which depends on the fracture toughness (G_i^c) as follows:

$$G^c = G_n^c + (G_s^c - G_n^c) \left\{ \frac{G_S}{G_T} \right\}^\eta \qquad (8)$$
$$where \quad G_S = G_s + G_t \;\; and \;\; G_T = G_n + G_S$$

being G_n, G_s and G_t the released rates energies in the three aforementioned directions, G_n^c and G_s^c the critical values of the released rates energies and η a parameter of the model (further detail could be found in the software documentation [23]). Material properties and model parameters are detailed in table 2.

2.3. Element erosion

The modified Hashin and Rotem model, used to describe the intra-laminar failure, has a built-in feature to remove elements from the mesh when either one damage variables associated with fibre failure modes (tensile or compressive) reaches the unity. When a unidirectional fragment with a quasi-isotropic layup impacts against a rigid plate, some of the layers will fail under matrix compression and hence the elements will not be removed promoting an excessive distortion and possible numerical problems. To solve this difficulty, a user subroutine was developed to define when a element should be removed prior to present excessive distortions; to this end the VUSDFLD subroutine from

Abaqus/Explicit was used. This subroutine, written in Fortran, allows the definition of field variables, being one of them the status of the finite element (active or not). The objective of this subroutine is to remove the element when it is completely damaged and hence without the capability of carry any load. If it is not removed, the element suffers excessive strain and distortion. Therefore a limit in the equivalent strain $\varepsilon_{eq} \geq 0.15$ was defined. This value is high enough to assure that the element is completely damaged and does not interfere in the material behaviour (It has to be noted that the composite laminates maximum strains are approximately 0.03).

3. Experimental tests for model validation

3.1. Experimental procedure

Experimental impact tests at high velocity of composite fragments against a rigid plate were performed in order to validate the numerical model presented in this work. The composite fragments were manufactured in autoclave using prepregs made by Hexcel Composites with AS4 carbon fibres and 8552 epoxy matrix. The thickness of the laminate was 4 mm (21 plies) and the ply sequence $(45/-45/90/0/90/-45/45/90/0/90/0)_{s'}$. The impactor size was $42 \times 100\, mm \times mm$. In order to accelerate the composite fragments, a 60 mm calibre pneumatic launcher was used; this experimental device uses compressed air (up to 6 bar) to impel the projectile. A sabot was used to guide the fragment through the 18 meters long canon. All the impact process was recorded using three high speed cameras. One of them was configured to perform a tracking of the fragment during the impact process and obtain the displacement-time curve; this curve will be used later to estimate the force-time history of the impactor.

Fragments were impacted in the direction of the 0°; the impact velocity range was between 70 to 180 m/s. The smallest value in the velocity range corresponds to almost no damage in the fragment whereas the highest produces

a considerable amount of failure. Further details of how the experimental tests were performed could be found in a previous work [20].

3.2. Experimental results

All the composite fragments showed a similar failure pattern. The face impacted is opened during the impact, showing a double cantilever beam opening process with an important erosion (see figure 2)[20]. The opening process is linked to delamination failure and the erosion is linked to matrix and fibre failure under compression (depending on the orientations of the plies). Once impacted, the erosion of the fragment is measured in order to quantify this value and use it for the model validation.

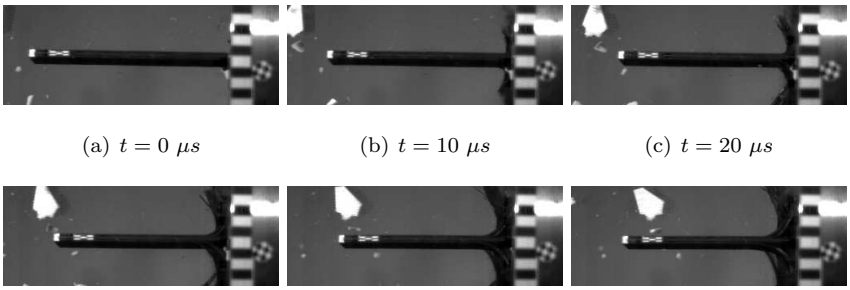

(a) $t = 0\ \mu s$ (b) $t = 10\ \mu s$ (c) $t = 20\ \mu s$

(d) $t = 30\ \mu s$ (e) $t = 40\ \mu s$ (f) $t = 50\ \mu s$

Figure 2: Sequence of the fragment impact at velocity of 103 m/s.[20]

The force induced during the impact is an important variable, since it will help in the design of structures that could withstand this type of loadings. The contact force is measured using the linear momentum balance of the whole fragment:

$$dt\, F = d\,(m\, v) = dm\, v + dv\, m \tag{9}$$

where F is the contact force, m is the fragment mass (that could vary during the impact process) and v the fragment velocity. In order to determine the evo-

lution of the fragment mass, it is assumed a linear decrement with the fragment position:

$$m\left(x\right) = \left(m_i - \frac{m_i - m_f}{x_f} x\left(t\right)\right) \tag{10}$$

where m_i is the initial mass, m_f is the final mass, x is the fragment displacement, and x_f is its final displacement. Then the Eq. 9 could be written as:

$$F\left(t\right) = \frac{dv\left(t\right)}{dt}\left(m_i - \frac{m_i - m_f}{x_f} x\left(t\right)\right) - v^2\left(t\right)\ \frac{m_i - m_f}{x_f} \tag{11}$$

where $\frac{dv}{dt}$ is the fragment acceleration. The two variables indicated in this section (the eroded distance and the force-time history) will be used in order to validate the numerical methodology presented in this work.

4. Numerical methodology

4.1. Finite element model

The finite element mesh used to model the composite laminate uses continuum shell plane stress elements with reduced integration (SC8R in Abaqus notation). The element size was constant along the geometry being its size $1 \times 1 \times 0.1905\ mm^3$ (small enough to avoid any snap-back in the stress-strain curve); a total of 4200 elements were used for each ply. The fragment uses 21 elements and 20 cohesive interactions through the thickness (88200 elements in total); Figure 3 shows the detail of the used mesh, which has been obtained after a refined process, achieving a good balance between results and computational cost.

A rigid plate, equal to the one used in the experiments, was defined to receive the impact. Since no deformation has been found in the experiments, a rigid solid behaviour was chosen. A spring which is clamped in one of its sides, and connected to the rigid plate in the other one, is used to measure the contact

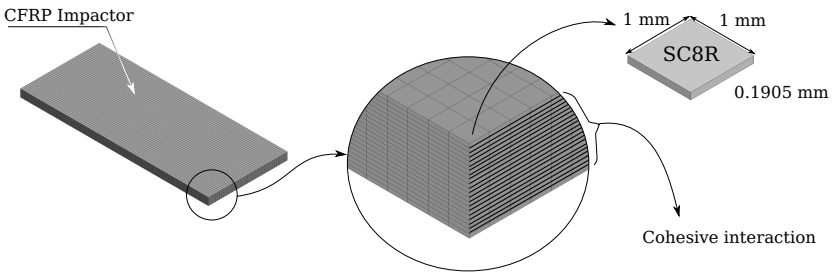

Figure 3: Finite element model of the fragment for the numerical simulation of impact.

force. Knowing the plate displacement, the contact force could be calculated as $F_c = m\,\ddot{x} + k\,x$, where m is the mass of the rigid plate and k is the spring rigidity. Figure 4 shows a sketch of the numerical simulation, including a linear spring, which is used to measure the impact force. The numerical load cell has been implemented because the contact force output variable could not be used due to the numerical noise produced by the contact algorithm and the erosion of the fragment.

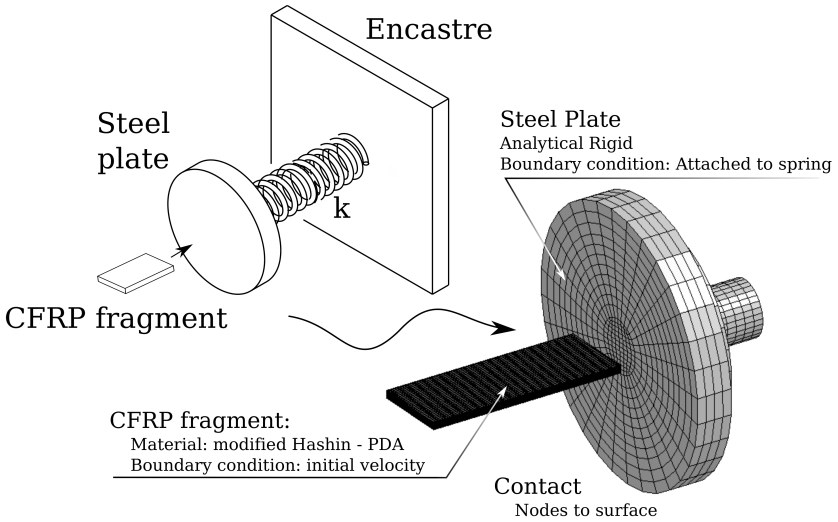

Figure 4: Sketch of the completely numerical model, including the spring k to measure the impact force.

5. Numerical results and validation

5.1. Kinematics

In order to validate the numerical methodology, the simulations were accomplished at different impact velocities ranging from 80 to 160 m/s. The first variable used to validate the model was the velocity history of the fragment during the impact; figure 5 shows the evolution of the velocity of the composite fragment at 140 m/s for both experimental and numerical results. The two curves are almost identical, showing the same trend. Firstly a sudden deceleration as soon as the fragment impacts the rigid plate decreasing almost to the half of the velocity in the first 0.1 ms, then the slope starts to be more gentle. This stepper zone corresponds to the beginning of the impact in which the aforementioned double cantilever beam is still not developed, as soon as it appears the deceleration starts to decrease. The agreement between the experimental and numerical values indicates that the overall behaviour of the fragment is well reproduced by the numerical methodology proposed in this work. This may lead to think that the erosion process that governs the kinematics of the composite could be well captured.

5.2. Erosion

Once it is shown that the kinematic behaviour of the fragment during the impact is similar, the erosion of the fragment (obtained numerically) is going to be compared both qualitative and quantitatively with the experimental results. Figure 6 shows the experimental and numerical images of the fragment impacted at 95 m/s. The erosion measured in the experimental results (9 mm) is well predicted by the numerical simulations. In addition it can be observed how the most exterior plies suffer a bigger delamination due to the double-cantilever opening process, which is partially captured by the numerical simulations. It is worth to mention that the numerical results correspond to an instant after the impact ends, so that the exterior plies have not recovered its initial position. According to the image, it could be considered that the model is able

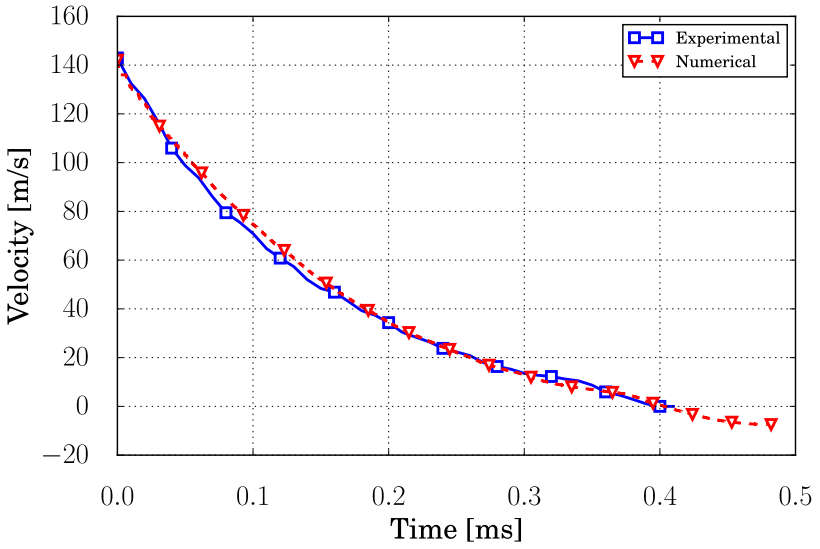

Figure 5: Evolution of the velocity of the composite fragment for both numerical and experimental results in a 143 m/s impact.

to reproduce adequately the main characteristics of erosion of the real fragment.

The images obtained experimentally during the impact process, by means of the high speed cameras, have been used to compare qualitatively the numerical results. Figure 7 shows the comparison of the frames during the impact in the first 500 μs. It is observed that in the firsts frames the double cantilever beam is not developed, which corresponds to the stepper deceleration of figure 5. Afterwards it can be observed the opening and erosion process. Although the double cantilever beam process is less wider in the numerical simulations and the final part of the opening seems to be under-predicted, it can be considered that the main stages of the whole impact and erosion process of the fragment are qualitatively well captured by the model.

In order to analyse the prediction capacity of the model, Figure 8 depicts the eroded distance for both experimental and numerical results as a function of

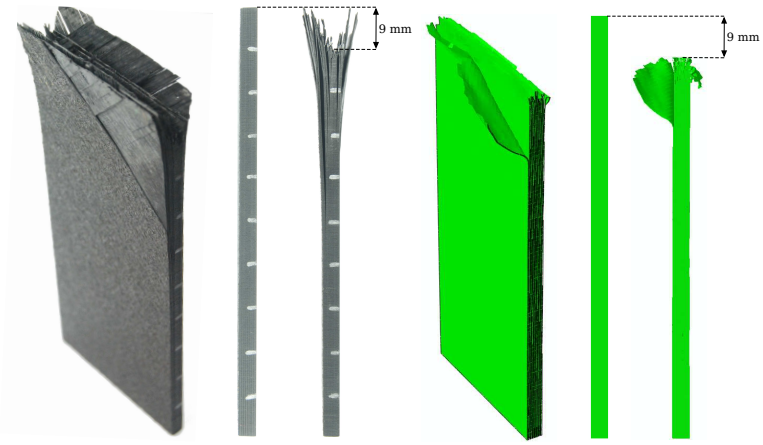

(a) Experimental (b) Numerical

Figure 6: Image showing the fragment erosion impacted at 95 m/s

the impact velocity. The figure shows the same trend behaviour regarding the eroded distance. As the impact velocity increases, the eroded distance raises; the higher the impact energy the larger the erosion. In spite of the small differences at low and high impact velocities, it could be considered that the model is able to reproduce adequately the erosion process and the distance eroded in a wide range of impact velocities.

The measurement of the eroded distance in the experimental specimens presents some uncertainty because of the roughness of the surfaces generated by the erosion. Therefore, it has been done another comparison taking into account the mass lost during the impact. The fragment weight before the impact is $\sim 26\,g$. After every test the fragments were weighed using a precise balance, and in the numerical simulations the final weight was calculated at the end of the impact. Figure 9 shows the percentage of mass lost during the impact for both numerical and experimental results, as a function of the impact velocity. In this case the numerical simulations overestimate slightly the experimental results. This was something expected taking into account the images of the numerical simulation shown in Figure 6 and Figure 7. As it has been already

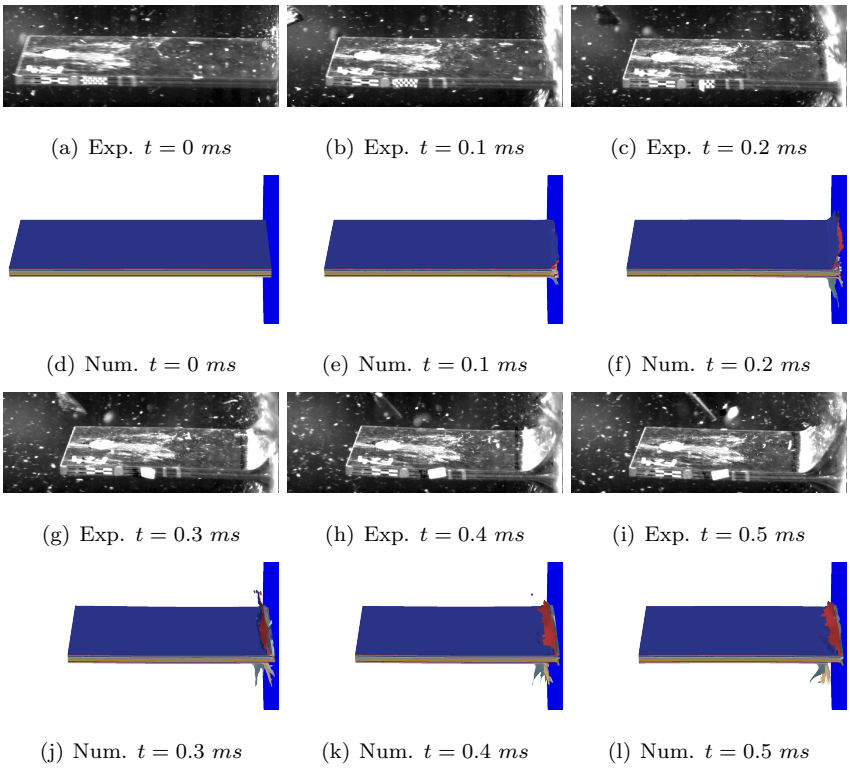

(a) Exp. $t = 0\ ms$ (b) Exp. $t = 0.1\ ms$ (c) Exp. $t = 0.2\ ms$

(d) Num. $t = 0\ ms$ (e) Num. $t = 0.1\ ms$ (f) Num. $t = 0.2\ ms$

(g) Exp. $t = 0.3\ ms$ (h) Exp. $t = 0.4\ ms$ (i) Exp. $t = 0.5\ ms$

(j) Num. $t = 0.3\ ms$ (k) Num. $t = 0.4\ ms$ (l) Num. $t = 0.5\ ms$

Figure 7: Comparison between numerical and the experimental results for an impact at 143 m/s

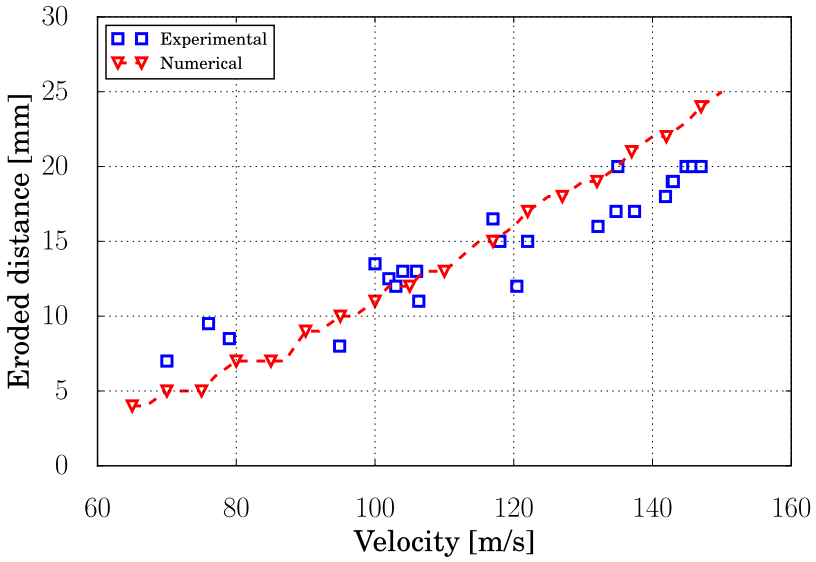

Figure 8: Eroded distance vs. impact velocity for both numerical and experimental results.

commented, the length of the double cantilever beam generated experimentally is under predicted by the numerical simulations. This fact has not a great influence into the eroded distance but the percentage of mass lost is bigger than experimentally. The lost of mass of the laminates due to the crack of the outer plies can also be observed in other numerical works related to crashworthiness [19] and it is something to improve in the models used to simulate this kind of impacts. Taking into account the numerical results, it seems that the model is able to reproduce properly the kinematic of the fragment and the eroded distance, nevertheless overestimates the mass lost. Therefore it is important to know if this overestimation could affect the force transmitted by the fragment. From a designer point of view an important parameter to design damage tolerant structures is the load applied during the impact, thus a good prediction of this parameter should be a desirable benchmark for the numerical model.

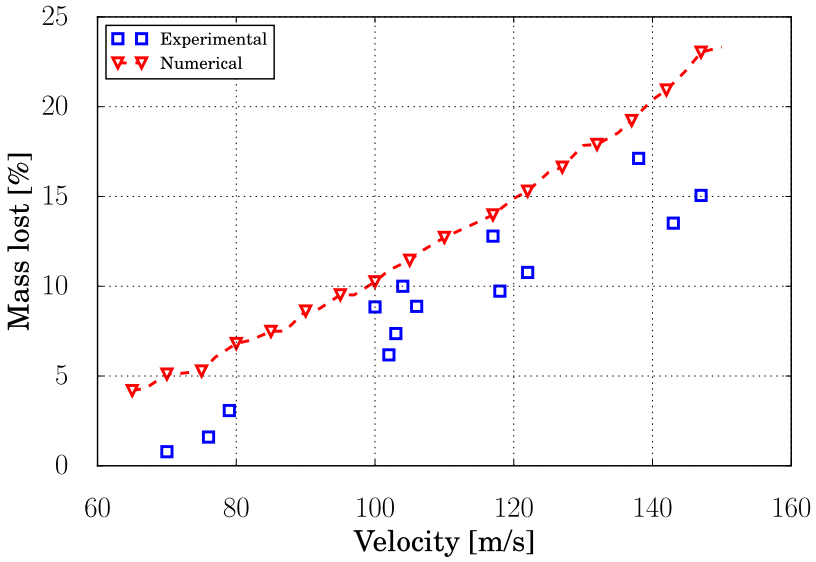

Figure 9: Percentage of mass lost vs. impact velocity for both numerical and experimental results.

5.3. Force and impulse

Force histories, measured and predicted by the numerical simulations, for four different impact velocities are depicted in Figure 10. It is shown that all the trends are similar; a stepper slope until the maximum peak and then a gentle slope until reaching a value next to zero [20]. It is observed that as the impact velocity increases, the peak force raises from 15 to more than 20 kN for an impact range velocity from 75 to 160 m/s respectively, as it was expected. Although the numerical simulation for the impact around 75 m/s shows some differences after the peak value, it can be said that in general the model is able to reproduce the peak force values and the trends observed experimentally reasonably well in a wide impact velocity range. As it has been said before, this fact is of great importance to design damage tolerant structures. In addition, taking into account this results it could be said that the overestimation of the mass lost previously commented has not a great influence in the force transmitted by the fragment.

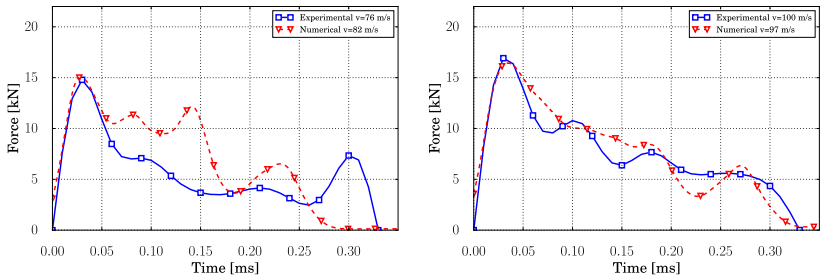

(a) $v \sim 75\ m/s$ (b) $v \sim 100\ m/s$

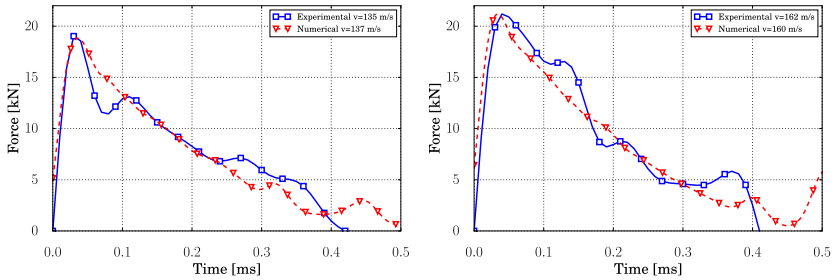

(c) $v \sim 135\ m/s$ (d) $v \sim 160\ m/s$

Figure 10: Experimental and numerical force histories.

Finally the impulse generated by the impact is analysed, this variable links the information of the magnitude of the force and its time history evolution. In Figure 11 is depicted the impulse generated in the rigid plate by the CFRP fragment as a function of the impact velocity, for the experimental and numerical results. The data shows a positive trend, the increasing of the impact velocity produces a raise in the momentum of the projectile and hence in the impulse, ranging from around 2 to more than 4 $N \cdot s$ for the highest velocity considered. Similar values and trends are predicted by the numerical simulations.

The numerical results shown in this section: kinematic of the fragment, erosion, mass lost, force and impulse show that the proposed numerical methodology (a Hashin criteria with PDA and a deletion user subroutine) could be an appropriate approach for the problem under consideration. It has been seen

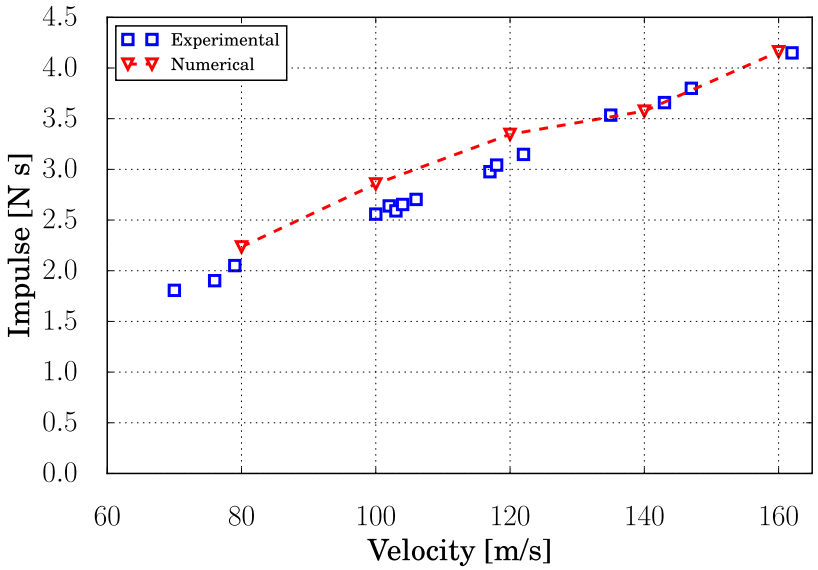

Figure 11: Impulse vs. impact velocity for both numerical and experimental results.

that the model overestimates the mass lost by the fragment. This is probably due to the use of 2D elements, which can produce an underestimation of the double cantilever beam damage process. This could be improved by using other kind of elements or taking into account another failure mechanism which would increase the computational cost. Nevertheless, the methodology proposed could be useful to perform some previous designs because the force and the impulse suffered by the target, in this case the rigid plate, are barely influenced by the overestimation of the mass lost by the fragment.

6. On the influence of the impact misalignment

The experimental setup used to impel the composite fragment against the rigid target could produce small changes in the misalignment of the composite slab. This uncertainty is unable to be measured properly using the images because it is too small, around $\pm 2^{\circ}$rotation degrees with respect to the target surface. This misalignment can not be studied experimentally since it is quite difficult to assure an exact angle out of the perpendicularity. Therefore the

validated model has been used to perform a study about the influence of the rotation angles. The trajectory of the fragment is kept perpendicular to the plate and two different angles of misalignment are studied: the yaw and the pitch (see Figure 12); modifying its values from 0°to 5°.

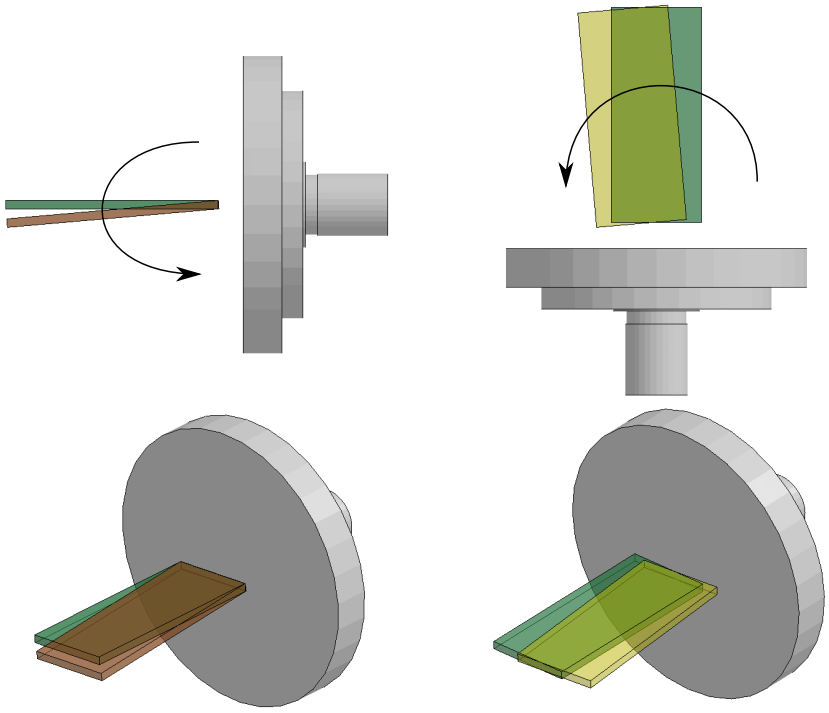

(a) Pitch (b) Yaw

Figure 12: Sketch of the angle variation: pitch and yaw.

The force time history curves for the misalignment cases are similar to the normal impacts, and also the kinematics of the fragment. In all the cases the double cantilever beam damage shape appear, even if the misalignment is 5°. In the following sections, the influence of the misalignment in the mass lost and the impulse is studied for different impact velocities and impact angles.

6.1. *Influence on the eroded mass*

The eroded mass can be quantified with the distance (aforementioned) or with the mass lost during the impact process. Since the second one is a more accurate measure, it is going to be selected to perform a comparison of how the variation of the yaw and pitch angle influences it. Figure 13 shows the numerical results of the eroded mass for different impact velocities (from 80 to 160 m/s) as a function of different pitch and yaw angles. As first approach it seems that there is no influence with the variation of the angles, except for the lower velocity case in which the differences are sensible. It is worth to note that at 80 m/s, as the angle increases, the eroded mass increases (for both pitch and yaw angles), but the influence is opposite when the impact velocity is higher.

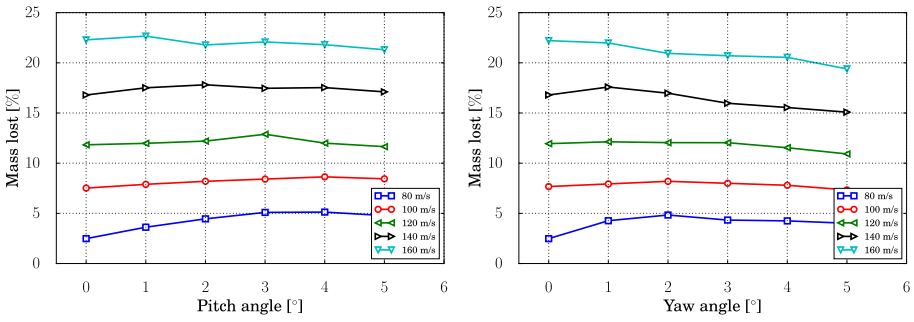

(a) Pitch (b) Yaw

Figure 13: Numerical results of eroded mass for different impact velocities and two angle variations left yaw, right pitch.

6.2. *Influence on the impulse*

The impulse generated by the impact is also analysed in this section. Figure 14 shows the numerical results of the impulse for different impact velocities (from 80 to 160 m/s) as a function of different pitch and yaw angles. It is clear that the angle does not influence sensibly the total impulse induced by the fragment. In the case of the yaw angle, the lines are almost horizontal, whereas for the pitch angle the differences are small and without a clear trend.

It could be stated that within the range of angles analysed in the present work, the impulse does not varies with the yaw and pitch angle.

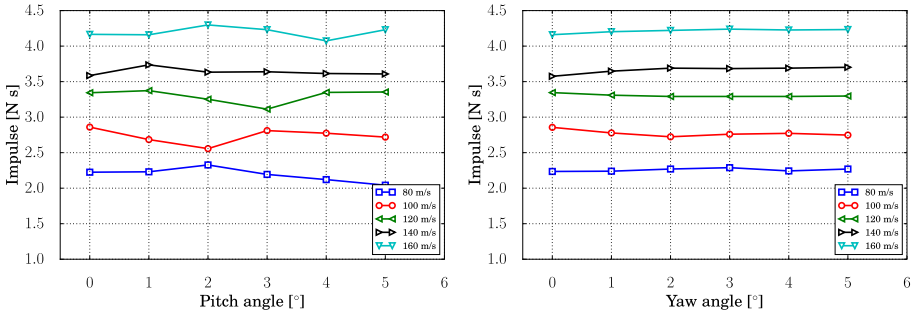

(a) Pitch (b) Yaw

Figure 14: Numerical results of eroded mass for different impact velocities and two angle variations left yaw, right pitch.

7. Conclusions

In this work the high velocity impact of composite fragments has been analysed. The study has been performed both from an experimental and a numerical point of view. Experimental tests have been performed by means of a gas gun, and the impact process has been recorded using a high speed video camera; the images obtained allowed to measure the deceleration of the fragment and hence the force and the impulse induced. An analysis of the failure process has also been performed using the impacted specimens. The numerical methodology proposed, uses a commercial finite element program and also a user subroutine specially developed to avoid excessive mesh distortions. Once validated, the numerical model has been used to study the influence of the fragment misalignment. From the results presented and discussed, the main conclusions extracted are:

- The composite fragment, when impacted at high velocity against a rigid plate, fails promoting a double cantilever beam shape. The main failure

mechanism that appear are the matrix and the fibre compression, as well as the delamination.

- A numerical methodology based on the Hashin model and a user subroutine has been developed in order to predict the force induced by the fragment during the impact and its erosion (both distance and mass). The results show a good correlation between experimental and numerical results.

- Once validated, the numerical model has been used for virtual testing. The misalignment variation has been studied, both pitch and yaw. The eroded mass and the impulse have been compared for angles up to 5°, observing that under these circumstances the influence on the aforementioned variables was insignificant.

Acknowledgements

This research was done with the financial support of the Spanish Ministry of Economy and Competitiveness (under projects DPI2013-41094-R and DPI2017-85073-R) and the Vicerrectorado de Política Científica of the Universidad Carlos III de Madrid (project numbers 2013/00413/002, 2013/00413/003 and 2014/00006/002).

References

[1] W. Cantwell, J. Morton, Geometrical effects in the low velocity impact response of CFRP, Composite Structures 12.

[2] W. Cantwell, J. Morton, Detection of impact damage in CFRP laminates, Composite Structures 3 (1985) 241–257.

[3] W. Cantwell, J. Morton, Comparison of the low and high velocity impact response of cfrp, Composites 20 (1989) 545–51.

[4] D. Medina, J. Chen, Three-dimensional simulations of impact induced damage in composite structures using the parallelized sph method, Composites Part A: Applied Science and Manufacturing 31 (8) (2000) 853 – 860.

[5] A. Johnson, M. Holzapfel, Influence of delamination on impact damage in composite structures, Composites Science and Technology 66 (6) (2006) 807 – 815, advances in statics and dynamics of delamination.

[6] S. Yashiro, K. Ogi, A. Yoshimura, Y. Sakaida, Characterization of high-velocity impact damage in cfrp laminates: Part ii - prediction by smoothed particle hydrodynamics, Composites Part A: Applied Science and Manufacturing 56 (2014) 308 – 318.

[7] J. López-Puente, R. Zaera, C. Navarro, High energy impact on woven laminates, J. Phys. IV 110 (110) (2003) 639–44.

[8] J. López-Puente, S. Li, Analysis of strain rate sensitivity of carbon/epoxy woven composites, International Journal of Impact Engineering 48 (2012) 54 – 64.

[9] J. Pernas-Sánchez, J. Artero-Guerrero, J.Zahr Viñuela, D. Varas, J. López-Puente, Numerical analysis of high velocity impacts on unidirectional laminates, Composite Structures 107 (2014) 629 – 634.

[10] J. López-Puente, R. Zaera, C. Navarro, Experimental and numerical analysis of normal and oblique ballistic impacts on thin carbon/epoxy woven laminates, Composites Part A: Applied Science and Manufacturing 39 (2) (2008) 374–387.

[11] D. Fernández-Fdz, J. López-Puente, R. Zaera, Prediction of the behaviour of cfrps against high-velocity impact of solids employing an artificial neural network methodology, Composites Part A: Applied Science and Manufacturing 39 (6) (2008) 989 – 996.

[12] D. Varas, J. Artero-Guerrero, J. Pernas-Sánchez, J. López-Puente, Analysis of high velocity impacts of steel cylinders on thin carbon/epoxy woven laminates, Composite Structures 95 (2013) 623–629.

[13] J. Pernas-Sánchez, J. Artero-Guerrero, D. Varas, J. López-Puente, Experimental analysis of ice sphere impacts on unidirectional carbon/epoxy laminates, International Journal of Impact Engineering 96 (2016) 1 – 10.

[14] J. Artero-Guerrero, J. Pernas-Sánchez, D. Varas, J. López-Puente, Numerical analysis of cfrp fluid-filled tubes subjected to high-velocity impact, Composite Structures 96 (2013) 286 – 297.

[15] J. Artero-Guerrero, J. Pernas-Sánchez, J. López-Puente, D. Varas, On the influence of filling level in CFRP aircraft fuel tank subjected to high velocity impacts., Composite Structures 107 (2014) 570–77.

[16] A. Mamalis, K. Spentzas, D. Papapostolou, N. Pantelelis, Finite element investigation of the influence of material properties on the crushing characteristics of in-plane loaded composite sandwich panels, Thin-Walled Structures 63 (2013) 163 – 174.

[17] A. Mamalis, D. Manolakos, M. Ioannidis, D. Chronopoulos, P. Kostazos, On the crashworthiness of composite rectangular thin-walled tubes internally reinforced with aluminium or polymeric foams: Experimental and numerical simulation, Composite Structures 89 (3) (2009) 416 – 423.

[18] H. Israr, S. Rivallant, J. Barrau, Experimental investigation on mean crushing stress characterization of carbon epoxy plies under compressive crushing mode, Composite Structures 96 (2013) 357–364.

[19] H. Israr, S. Rivallant, C. Bouvet, J. Barrau, Finite element simulation of 0/90 cfrp laminated plates subjected to crushing using a free-face-crushing concept, Composites Part A: Applied Science and Manufacturing 62 (2014) 16–25.

[20] A. Mata-Díaz, J. López-Puente, D. Varas, J. Pernas-Sánchez, J. Artero-Guerrero, Experimental analysis of high velocity impacts of composite fragments, International Journal of Impact Engineering 103 (2017) 231 – 240.

[21] Z. Hashin, A. Rotem, A cumulative damage theory of fatigue failure, Materials Science and Engineering 34 (2) (1978) 147–160.

[22] P. Camanho, C. Davila, Mixed-mode decohesion finite elements for the simulation of delamination in composite materials, Nasa/tm-2002-211737 2002;1-37., NASA (2002).

[23] ABAQUS version 6.14 online documentation. Analysis user's manual. Simulia Inc. Dassault Systèmes, 2013.

[24] Z. Hashin, A. Rotem, A fatigue failure criterion for fiber reinforced materials, Tech. rep., Department of materials engineering; Technion - Israel institute of technology, Haifa, Israel (1973).

[25] A. Matzenmiller, J. Lubliner, R. Taylor, A constitutive model for anisotropic damage in fiber-composites, Mechanics of Materials 20 (2) (1995) 125 – 152.

[26] J. Pernas-Sánchez, J. Artero-Guerrero, J. López-Puente, D. Varas, Numerical methodology to analyze the ice impact threat: Application to composite structures, Materials & Design 141 (2018) 350 – 360.

[27] C. Lopes, Z. Gurdal, P. Camanho, P. Maimi, E. Gonzalez, Simulation of low-velocity impact damage on composite laminates, Structures, Structural Dynamics, and Materials and Co-located Conferences, American Institute of Aeronautics and Astronautics, 2009.

[28] A. Turon, P. Camanho, J. Costa, C. Dávila, A damage model for the simulation of delamination in advanced composites under variable-mode loading, Mechanics of Materials 38 (11) (2006) 1072–1089.

[29] M. Benzeggagh, M. Kenane, Measurement of mixed-mode delamination fracture toughness of unidirectional glass/epoxy composites with mixed-mode bending apparatus, Composites Science and Technology 56 (4) (1996) 439–449.